International Journal of Nanomedicine

Dovepress
open access to scientific and medical research

Open Access Full Text Article

ORIGINAL RESEARCH

The theranostic efficiency of tumor-specific, pH-responsive, peptide-modified, liposome-containing paclitaxel and superparamagnetic iron oxide nanoparticles

This article was published in the following Dove Press journal:
International Journal of Nanomedicine

Xiu-Chai Zheng[1,2,*]
Wei Ren[1,2,*]
Shuang Zhang[1,2]
Ting Zhong[1,2]
Xiao-Chuan Duan[1,2]
Yi-Fan Yin[1,2]
Mei-Qi Xu[1,2]
Yan-Li Hao[1,2]
Zhan-Tao Li[1,2]
Hui Li[1,2]
Man Liu[1,2]
Zhuo-Yue Li[1,2]
Xuan Zhang[1,2]

[1]Beijing Key Laboratory of Molecular Pharmaceutics and New Drug Delivery Systems, School of Pharmaceutical Sciences, Peking University, Beijing, People's Republic of China; [2]Department of Pharmaceutics, School of Pharmaceutical Sciences, Peking University, Beijing, People's Republic of China

*These authors contributed equally to this work

Correspondence: Xuan Zhang
Department of Pharmaceutics, School of Pharmaceutical Sciences, Peking University, Xueyuan Road 38, Beijing 100191, People's Republic of China
Tel/fax +86 10 8280 5928
Email xuanzhang@bjmu.edu.cn

Background: In the present study, the tumor-specific, pH-responsive peptide $H_7K(R_2)_2$ -modified, theranostic liposome-containing paclitaxel (PTX) and superparamagnetic iron oxide nanoparticles (SPIO NPs), PTX/SPIO-SSL-$H_7K(R_2)_2$, was prepared by using $H_7K(R_2)_2$ as the targeting ligand, SPIO NPs as the magnetic resonance imaging (MRI) agent, PTX as antitumor drug.

Methods: The PTX/SPIO-SSL-$H_7K(R_2)_2$ was prepared by a thin film hydration method. The characteristics of PTX/SPIO-SSL-$H_7K(R_2)_2$ were evaluated. The targeting effect, MRI, and antitumor activity of PTX/SPIO-SSL-$H_7K(R_2)_2$ were investigated detail in vitro and in vivo in human breast carcinoma MDA-MB-231 cell models.

Results: Our results of in vitro flow cytometry, in vivo imaging, and in vivo MR imaging confirmed the pH-responsive characteristic of $H_7K(R_2)_2$ in MDA-MB-231 cell line in vitro and in vivo. The results of in vivo MRI and in vivo antitumor activity confirmed the theranostic effect of PTX/SPIO-SSL-$H_7K(R_2)_2$ in MDA-MB-231 tumor-bearing model.

Conclusion: Considering all our in vitro and in vivo results, we conclude that we developed targeting modified theranostic liposome which could achieve both role of antitumor and MRI.

Keywords: tumor-specific pH-responsive peptide, paclitaxel, superparamagnetic iron oxide nanoparticles, liposome, theranostic efficiency

Introduction

Theranostic nanomedicines possess diagnostic and therapeutic functions in one integrated system, having diagnosis, therapy, and monitoring of therapeutic response at the same time.[1,2] They can be used for various applications, such as chemotherapy, photodynamic therapy, siRNA therapy and photothermal therapy, pathologic progress monitoring, and prediction of therapeutic efficacy.[1]

Theranosis requires noninvasive imaging modalities including optical imaging, magnetic resonance imaging (MRI), computed tomography, and positron emission tomography.[3] Among them, MRI is one of most commonly used techniques. It involves no exposure to ionizing radiation, enables imaging with high spatial resolution, and provides high contrast in the soft tissue.[4] Many nanoparticles (NPs), including superparamagnetic iron oxide (SPIO), gold, silver, and other metals, are currently being investigated and used as contrast agents.

SPIO NPs are contrast agents that have a variety of applications in molecular and cellular MRI.[5–8]

Many efforts have been made to combine SPIO NPs and antitumor drugs within a single delivery system to achieve theranostic strategy.[9–12] SPIO NP-loaded liposomes

submit your manuscript | www.dovepress.com
Dovepress
http://dx.doi.org/10.2147/IJN.S157082

have gained much attention for their use in hyperthermia, MRI, magnetic targeting, and theranostic strategy.[13–18]

It is well known that solid tumor tissues are more acidic (pH 6.0–7.0) compared to the neutral surroundings of normal organs (pH 7.4). This acidic pH characteristic in the tumor tissues could be used as the targeting site.[19,20] It has been reported that many cell penetrating peptides (CPPs) respond to tumor acidic microenvironments, producing targeting activity.[21–24] In our previous study, we designed a tumor-specific, pH-responsive $H_7K(R_2)_2$, which could respond to the acidic pH in the tumor tissues.[23,24] This tumor-specific, pH-responsive $H_7K(R_2)_2$ could produce CPP characteristics at a low pH in tumor tissues and non-CPP characteristics at a normal pH in normal tissues.

Considering the effect of $H_7K(R_2)_2$ and SPIO NPs, in this study, $H_7K(R_2)_2$ was selected as the targeting ligand, SPIO NP as an MRI agent, and paclitaxel (PTX) as the antitumor drug to prepare the target modified theranostic PTX/SPIO-SSL-$H_7K(R_2)_2$. The targeting effect, MRI, and antitumor activity of PTX/SPIO-SSL-$H_7K(R_2)_2$ were investigated in detail in vitro and in vivo.

Materials and methods

Materials

Egg phosphatidylcholine was supplied by Lipoid GmbH (Ludwigshafen, Germany). DSPE-PEG_{2000} (DSPE-PEG) and DSPE-PEG_{2000}-NHS (DSPE-PEG-NHS) were obtained from NOF Corporation (Tokyo, Japan). Coumarin-6, cholesterol, sulforhodamine B, and tris base were bought from Sigma-Aldrich (St Louis, MO, USA). The Ac-RRK(HHHHHHH) RR-NH_2 peptide ($H_7K(R_2)_2$) was synthesized by Beijing Scilight Biotechnology Co., Ltd. (Beijing, China). DSPE-PEG-$H_7K(R_2)_2$ was synthesized by our laboratory according to a previously reported method.[23,24] PTX was obtained from Mei-Lian Co., Ltd. (Chongqing, China). Near-infrared lipophilic carbocyanine dye 1,10-dioctadecyltetramethyl indotricarbocyanine iodide (DiR) and coumarin-6 were supplied by Biotium, Inc. (Hayward, CA, USA).

SPIO NPs were synthesized by our lab according to the reported reference.[25]

The human breast carcinoma MDA-MB-231 cell line was obtained from the Chinese Academy of Sciences Cell Bank (Shanghai, China). This cell line was cultured according to the recommended instructions.

Animals

Female BALB/c nude mice (18–20 g) were supplied by the Experimental Animal Center of Peking University (Beijing, China). Animals were acclimatized for 7 days prior to the experiment and were allowed free access to a standard diet and water. The temperature and relative humidity were maintained at 25°C and 50%, respectively. This study was performed following the National Institutes of Health guidelines for the use of experimental animals; all care and handling of animals were performed with the approval of the Experimental Animal Center of Peking University Health Science Center.

Preparation of $H_7K(R_2)_2$-modified, PTX/SPIO-loaded liposomes

The $H_7K(R_2)_2$-modified, liposome-containing PTX and SPIO (PTX/SPIO-SSL-$H_7K(R_2)_2$) was prepared according to our previously reported method.[26] Briefly, a mixture of PTX, egg phosphatidylcholine, cholesterol, DSPE-PEG, and DSPE-PEG-$H_7K(R_2)_2$ was dissolved in chloroform and evaporated using an RE52 rotary evaporator (Shanghai Yarong Biochemistry Instrument Company, Shanghai, China) to obtain a solid film. To remove any traces of chloroform, this film was flushed with nitrogen gas and stored overnight in a desiccator. After that, the thin film was hydrated in a 5% glucose solution containing SPIO NPs by sonication in a water bath to obtain a suspension of liposomes. The liposome suspension was extruded 10 times through a polycarbonate membrane (EMD Millipore, Billerica, MA, USA) with a pore size of 100 nm. The free PTX and SPIO NPs were then separated on a Sephadex G-50 column by eluting with 5% glucose solution.

$H_7K(R_2)_2$-modified, liposome-containing PTX (PTX-SSL-$H_7K(R_2)_2$) was prepared by a similar procedure, except that 5% glucose solution was used as the hydration medium.

PTX/SPIO-loaded liposome (PTX/SPIO-SSL) was prepared by an identical procedure, except that an equivalent molar of DSPE-PEG-$H_7K(R_2)_2$ was replaced by DSPE-PEG.

Sterically stabilized liposome-containing PTX (PTX-SSL) was prepared by a similar procedure, except that the DSPE-PEG-$H_7K(R_2)_2$ replaced by DSPE-PEG and 5% glucose solution was used as the hydration medium.

The preparation of liposome loaded with coumarin-6 or DiR (coumarin-6-SSL, coumarin-6/SPIO-SSL, coumarin-6/SPIO-SSL-$H_7K(R_2)_2$; or DiR/SPIO-SSL, DiR/SPIO-SSL-$H_7K(R_2)_2$) was carried out by a similar procedure, except that the PTX was replaced by coumarin-6 or DiR.

Characterization of PTX/SPIO-SSL-$H_7K(R_2)_2$

The particle size and zeta potential of PTX/SPIO-SSL-$H_7K(R_2)_2$ were measured using a Malvern Zeta Sizer

Nano-ZS (Malvern Instruments, Malvern, UK) at 25°C. The encapsulation efficiency of PTX was estimated from the following formula:

$$\text{Encapsulation efficiency of PTX} = \frac{\text{PTX concentration in the filtered liposomes}}{\text{PTX concentration in the unfiltered liposomes}} \times 100\%$$

In vitro release of PTX from PTX/SPIO-SSL-$H_7K(R_2)_2$

The release of PTX from PTX/SPIO-SSL-$H_7K(R_2)_2$ was evaluated according to our previously reported mothed.[23] Briefly, a sample of PTX/SPIO-SSL-$H_7K(R_2)_2$ (0.4 mL, 0.5 mg/mL) was placed in a dialysis bag (MWCO 8,000–14,000 Da) and tightly sealed. Then, the dialysis bag was immersed in 200 mL release medium (PBS containing 0.1% [v/v] Tween 80) and incubated in an orbital shaker for 48 h at 37°C. Samples (0.2 mL) were taken at predetermined time intervals from the release medium over a period of 48 h, and these were replaced by a similar volume of fresh medium. The concentration of PTX was determined by high-performance liquid chromatography.[27]

Flow cytometry

The pH-responsive activity was evaluated in MDA-MB-231 cell line at pH 6.8 and pH 7.4 by using coumarin-6/SPIO-SSL-$H_7K(R_2)_2$ as a tracer. Briefly, MDA-MB-231 cells were seeded at a density of 3×10^5 cells/well in six-well plates and incubated at 37°C for 24 h to allow cell attachment. After 24 h, the medium was replaced with cell culture medium (pH 6.8 or pH 7.4) containing coumarin-6 solution or coumarin-6–loaded liposomes (the concentration of coumarin-6 was 100 ng/mL). After incubation for 2 h, the cells were washed three times with PBS solution. The cells were then harvested by trypsinization and centrifuged at 1,000 rpm for 5 min, resuspended in 500 mL PBS medium, and examined by flow cytometry using a FACScan instrument (Becton Dickinson, San Jose, CA, USA). Cell-associated coumarin-6 was excited with an argon laser (430 nm) and fluorescence was detected at 485 nm.[24]

In vitro cytotoxicity of PTX/SPIO-SSL-$H_7K(R_2)_2$

The in vitro antitumor activity of PTX/SPIO-SSL-$H_7K(R_2)_2$ was evaluated in MDA-MB-231 cell line following our previously reported method.[23,24,28–31] Briefly, MDA-MB-231 cells (1×10^4 cells/well) were seeded in 96-well plates and incubated for 24 h. Then, the cells were treated with cell culture medium (pH 6.8 or pH 7.4) containing different amounts of PTX-loaded liposomes and incubated for 48 h at 37°C. The cell viability was determined by sulforhodamine B assay.

Absorbance was measured at 540 nm using a 96-well plate reader (model 680; Bio-Rad Laboratories, Hercules, CA, USA). The survival percentages were calculated using the formula: survival % = (A_{540} nm for the treated cells/A_{540} nm for the control cells) ×100%, where A_{540} nm is the absorbance value. Each assay was carried out in triplicate. The IC_{50} values were calculated according to the dose–effect curves.

In vivo imaging in mice

The MDA-MB-231 tumor-bearing nude mice model was established by subcutaneous injection of 0.2 mL MDA-MB-231 cell suspension (5×10^6 cells) with 20% basement membrane matrix into the right leg of each female BALB/c nude mouse. Once the tumor masses reached ~200–300 mm^3 in volume, the mice received intravenous (i.v.) injection, via the tail vein, of 5% glucose, DiR/SPIO-SSL, or DiR/SPIO-SSL-$H_7K(R_2)_2$ at a dose of 800 ng/mouse. The mice were anesthetized by isoflurane (1.5%) and scanned at 2, 4, 6, 8, 24, and 48 h after administration using an IVIS® Spectrum in vivo imaging system (Xenogen, Inc., Alameda, CA, USA) with an excitation bandpass filter at 730 nm and an emission filter at 790 nm. The fluorescent signal intensities in the tumor-bearing mice were analyzed using Living Image 4.3 software (Caliper Life Sciences).

In vivo MRI in mice

The in vivo MR image of PTX/SPIO-SSL-$H_7K(R_2)_2$ was investigated in the MDA-MB-231 tumor-bearing nude mice. The MDA-MB-231 tumor-bearing nude mice model was established by subcutaneous injection of 0.2 mL MDA-MB-231 cell suspension (5×10^6 cells) with 20% basement membrane matrix into the right leg of each female BALB/c nude mouse. Once the tumor masses reached ~200–300 mm^3 in volume, the mice received i.v. injection, via the tail vein, of PTX/SPIO-SSL or PTX/SPIO-SSL-$H_7K(R_2)_2$ at a dose of 15 mg/kg PTX. After injection, MRI was conducted on a Bruker Biospec 70/20 scanner (Bruker BioSpin MRI, Ettlingen, Germany).

In vivo antitumor activity

The antitumor activity of PTX/SPIO-SSL-$H_7K(R_2)_2$ was investigated in the MDA-MB-231 tumor-bearing nude mice compared with PTX/SPIO-SSL and PTX-SSL. The MDA-MB-231 tumor-bearing nude mice model was established by

subcutaneous injection of 0.2 mL MDA-MB-231 cell suspension (5×10^6 cells) with 20% basement membrane matrix into the right leg of each female BALB/c nude mouse.[31] Once the tumor masses reached ~200–300 mm^3 in volume, the mice were randomly assigned to four groups (six animals per group): group I was given a 5% glucose solution, group II was given PTX-SSL (15 mg/kg, i.v., twice a day for 4 days [q4d]), group III was given PTX/SPIO-SSL (15 mg/kg, i.v., q4d), and group IV was given PTX/SPIO-SSL-$H_7K(R_2)_2$ (15 mg/kg, i.v., q4d). For all administrations, the formulations were given via the tail vein. The total dose of PTX in all treatment groups was 60 mg/kg. Throughout the study, mice were weighed and tumors were measured with calipers every 2 days. Tumor volumes were calculated from the formula: V = length (cm) × width^2 (cm^2) ×0.5236. On day 21 after tumor inoculation, one or two mice in each group were executed and the tumors were collected for the preparation of histologic sections. Terminal deoxynucleotidyl transferase dUTP nick end labeling staining of the frozen tissue sections was performed according to the standard protocols provided by the manufacturers.

Statistical analysis

Data are presented as the mean ± SD. One-way analysis of variance was used to determine significance among groups, after which post hoc tests with the Bonferroni correction were used for comparison between individual groups. Statistical significance was established at $p<0.05$.

Results

Preparation and characteristics of PTX/SPIO-SSL-$H_7K(R_2)_2$

The schematic diagram for preparation of PTX-SSL, PTX-SSL-$H_7K(R_2)_2$, PTX/SPIO-SSL, and PTX/SPIO-SSL-$H_7K(R_2)_2$ is illustrated in Figure 1. The particle size of PTX/SPIO-SSL-$H_7K(R_2)_2$ was 168.30±2.80 nm with a polydispersity of 0.197±0.015. The zeta potential of PTX/SPIO-SSL-$H_7K(R_2)_2$ was −10.50±0.44 mV, as shown in Table 1. The entrapment efficiency of PTX in PTX/SPIO-SSL-$H_7K(R_2)_2$ was >90%.

In vitro release of PTX from PTX/SPIO-SSL-$H_7K(R_2)_2$

The in vitro release of PTX from PTX-SSL, PTX/SPIO-SSL, and PTX/SPIO-SSL-$H_7K(R_2)_2$ in both pH 6.8 and 7.4 buffer solutions was investigated. As shown in Figure 2, the released PTX from PTX/SPIO-SSL-$H_7K(R_2)_2$ in both buffer solutions of pH 6.8 and 7.4 was almost identical (Figure 2C). Similar results were also observed in PTX-SSL and PTX/SPIO-SSL (Figure 2A and B).

Flow cytometry analysis

The in vitro targeting effect of $H_7K(R_2)_2$-modified coumarin-6 liposomes was investigated in MDA-MB-231 cells. The total coumarin-6 uptake by MDA-MB-231 cells from the coumarin-6 formulations was quantified by using flow cytometry. As shown in Figure 3, the level of cellular coumarin-6 for coumarin-6-SSL and coumarin-6/SPIO-SSL at pH 6.8 and 7.4 was almost similar. In addition, at pH 7.4, the intense fluorescence of coumarin-6 for coumarin-6-SSL, coumarin-6/SPIO-SSL, and coumarin-6/SPIO-SSL-$H_7K(R_2)_2$ was also almost identical. However, at pH 6.8, the cellular coumarin-6 level for coumarin-6/SPIO-SSL-$H_7K(R_2)_2$ was about 1.5-fold higher than that at pH 7.4.

In vitro cytotoxicity of PTX-SSL-$H_7K(R_2)_2$

The in vitro cytotoxicity of PTX-SSL-$H_7K(R_2)_2$ in MDA-MB-231 cell line was investigated. The IC_{50} values of PTX-SSL-$H_7K(R_2)_2$ and PTX-SSL groups were almost identical at pH 7.4 (Table 2). However, the IC_{50} value of the PTX-SSL-$H_7K(R_2)_2$ group at pH 6.8 (7.24±0.57 μM), unlike the PTX-SSL group, was significantly reduced, compared with that at pH 7.4 (31.97±4.94 μM).

In vivo imaging in MDA-MB-231 tumor model

The in vivo targeting effect of $H_7K(R_2)_2$-modified DiR liposomes was evaluated in MDA-MB-231 tumor-bearing mice. The tumor distribution of fluorescent DiR in MDA-MB-231 tumor-bearing mice is shown in Figure 4A. Our results indicated that the DiR fluorescence signal at the tumor site for the mice treated with DiR/SPIO-SSL-$H_7K(R_2)_2$ was stronger than in those treated with DiR/SPIO-SSL at all observed time points.

In vivo MRI in MDA-MB-231 tumor model

The in vivo targeting effect of PTX/SPIO-SSL-$H_7K(R_2)_2$ was also investigated in MDA-MB-231 tumor-bearing mice by MRI. MRI was performed on the MDA-MB-231 tumor-bearing mice before and after i.v. injection of PTX/SPIO-SSL and PTX/SPIO-SSL-$H_7K(R_2)_2$. Figure 4B shows a coronal view of tumor slices, where the tumor appears white on T_2-weighted images before injection of liposomes. A signal decrease of tumor along with time was observed in the

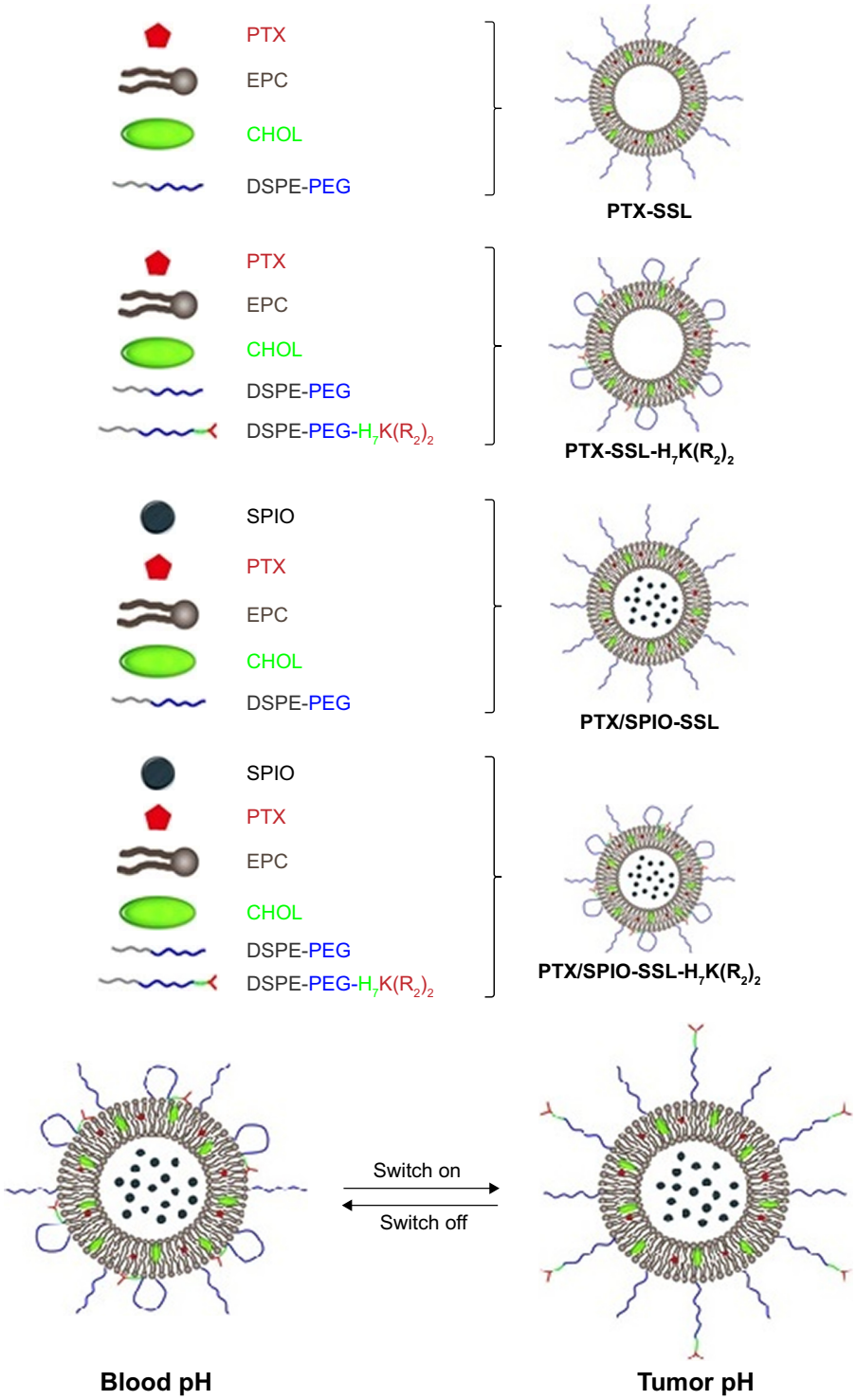

Figure 1 The schematic diagram for preparation of PTX-SSL, PTX-SSL-$H_7K(R_2)_2$, PTX/SPIO-SSL, and PTX/SPIO-SSL-$H_7K(R_2)_2$.
Abbreviations: CHOL, cholesterol; EPC, egg phosphatidylcholine; PEG, polyethylene glycol; PTX, paclitaxel; PTX/SPIO-SSL, PTX/SPIO-loaded liposome; PTX/SPIO-SSL-$H_7K(R_2)_2$, $H_7K(R_2)_2$-modified liposome containing PTX and SPIO; PTX-SSL, sterically stabilized liposome containing PTX; SSL, sterically stabilized liposome; SPIO, superparamagnetic iron oxide.

mice treated with PTX/SPIO-SSL-$H_7K(R_2)_2$. But there was no significant change of signal in the tumor of mice treated with PTX/SPIO-SSL. The quantitative analysis of T_2 values of the tumors was also performed. Our results indicated that the greatest T_2 value decrease of PTX/SPIO-SSL group was only 13%±12% observed at 0.5 h, while 28%±6% decrease of PTX/SPIO-SSL-$H_7K(R_2)_2$ group was observed at the same time (Figure 4C). The greatest T_2 value decrease of

Table 1 The characterization of PTX/SPIO-SSL-$H_7K(R_2)_2$ (n=3)

Formulations	Size (nm)	PDI	Zeta potential (mV)
PTX-SSL	159.20±2.03	0.132±0.006	−13.47±0.61
PTX/SPIO-SSL	167.07±0.95	0.218±0.006	−11.33±0.75
PTX/SPIO-SSL-$H_7K(R_2)_2$	168.30±2.80	0.197±0.015	−10.50±0.44

Abbreviations: PDI, polydispersity index; PTX, paclitaxel; PTX/SPIO-SSL, PTX/SPIO-loaded liposome; PTX/SPIO-SSL-$H_7K(R_2)_2$, $H_7K(R_2)_2$-modified liposome containing PTX and SPIO; PTX-SSL, sterically stabilized liposome containing PTX; SSL, sterically stabilized liposome; SPIO, superparamagnetic iron oxide.

PTX/SPIO-SSL-$H_7K(R_2)_2$ group at 1.5 h was 30%±3%. These results indicated that the in vivo MR image of PTX/SPIO-SSL-$H_7K(R_2)_2$ group was significantly superior to that of PTX/SPIO-SSL.

In vivo antitumor activity

The antitumor effect of PTX/SPIO-SSL-$H_7K(R_2)_2$ was evaluated in MDA-MB-231 tumor-bearing mice. The tumor growth was significantly inhibited in all treatment groups compared with the control group given 5% glucose solution ($p<0.01$), but the effect varied (Figure 5A). The antitumor activities of PTX-SSL and PTX/SPIO-SSL had no significant statistical differences. PTX/SPIO-SSL-$H_7K(R_2)_2$ significantly inhibited the growth of MDA-MB-231 tumors compared with that in the PTX-SSL and PTX/SPIO-SSL treatment groups ($p<0.01$). The mean tumor size at day 31 after implantation in the PTX-SSL, PTX/SPIO-SSL, and PTX/SPIO-SSL-$H_7K(R_2)_2$ groups was 531±128, 493±154, and 177±85 mm^3,

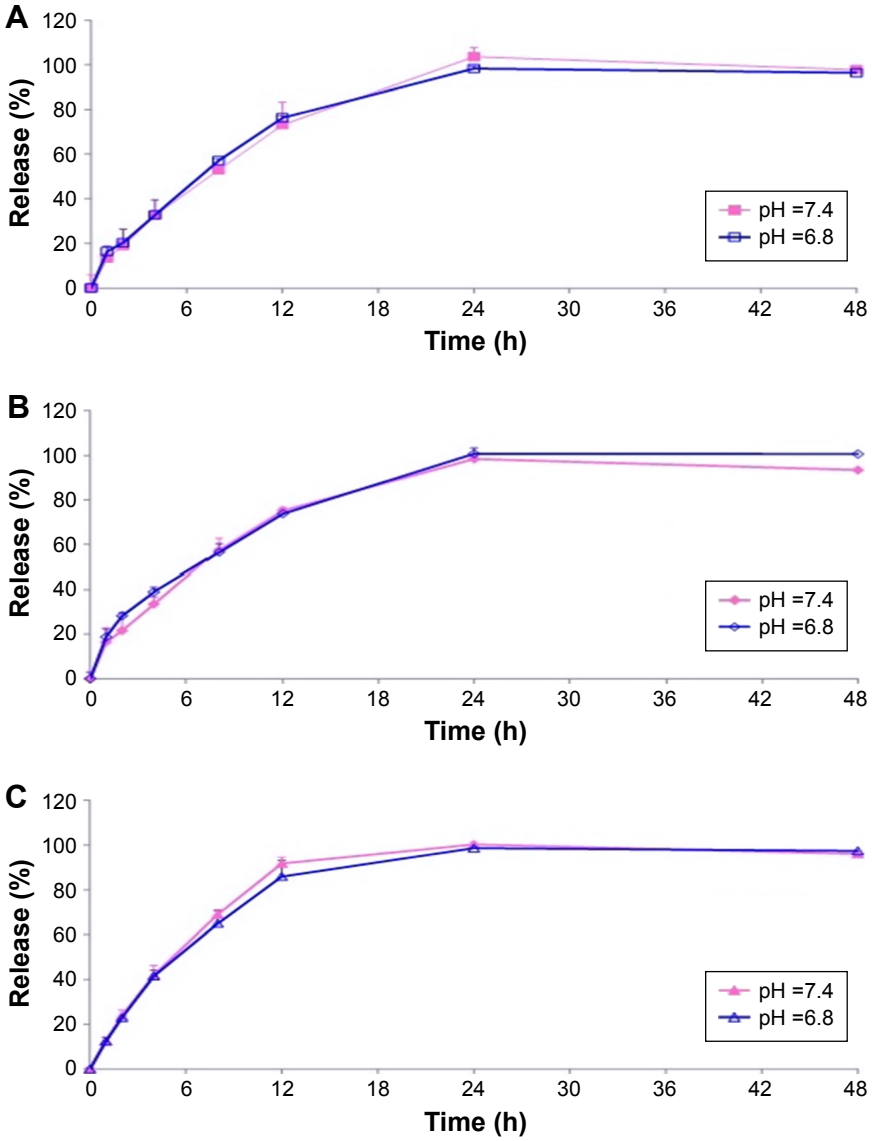

Figure 2 In vitro release of PTX from PTX-SSL, PTX/SPIO-SSL, and PTX/SPIO-SSL-$H_7K(R_2)_2$ at 37°C in pH 6.8 and 7.4 PBS buffer medium, respectively.
Notes: Data represent the mean ± SD (n=3). (**A**) PTX-SSL; (**B**) PTX/SPIO-SSL; (**C**) PTX/SPIO-SSL-$H_7K(R_2)_2$.
Abbreviations: PTX, paclitaxel; PTX/SPIO-SSL, PTX/SPIO-loaded liposome; PTX/SPIO-SSL-$H_7K(R_2)_2$, $H_7K(R_2)_2$-modified liposome containing PTX and SPIO; PTX-SSL, sterically stabilized liposome containing PTX; SSL, sterically stabilized liposome; SPIO, superparamagnetic iron oxide.

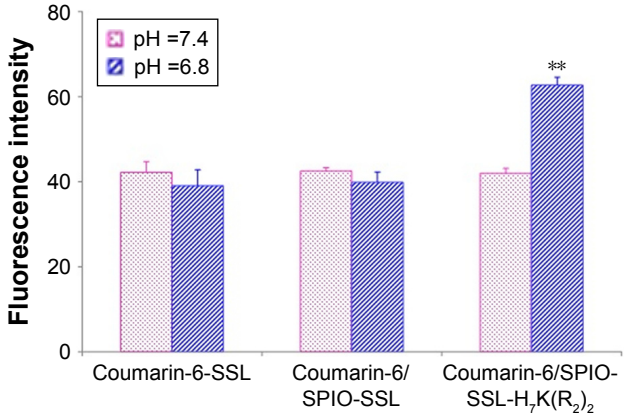

Figure 3 The flow cytometric measurement.
Notes: Flow cytometric measurement of coumarin-6 uptake from coumarin-6-SSL, coumarin-6/SPIO-SSL, or coumarin-6/SPIO-SSL-$H_7K(R_2)_2$ by MDA-MB-231 cells (n=3). **$p<0.01$ versus that at pH 7.4.
Abbreviations: SPIO, superparamagnetic iron oxide; SSL, sterically stabilized liposome.

respectively, compared with 1,768±614 mm^3 in the control group. The corresponding tumor growth inhibition in the PTX-SSL-, PTX/SPIO-SSL-, and PTX/SPIO-SSL-$H_7K(R_2)_2$-treated groups was about 70%, 70%, and 90%, respectively. The antitumor activity of Taxol in MDA-MB-231 tumor-bearing nude mice was also investigated in this research. Our results indicated that the tumor growth inhibited in Taxol treatment group was similar to that in PTX/SPIO-SSL-$H_7K(R_2)_2$ treatment group (data not shown).

The effect of tumor cell apoptosis was also evaluated by terminal deoxynucleotidyl transferase dUTP nick end labeling analysis staining of tumor tissue sections. Tumors of the PTX/SPIO-SSL-$H_7K(R_2)_2$-treated group exhibited more advanced cell apoptosis compared with the groups treated with 5% glucose solution, PTX-SSL, and PTX/SPIO-SSL ($p<0.01$), as shown in Figure 5B and C.

Discussion

Here, we selected $H_7K(R_2)_2$ as the targeting ligand, SPIO NP as the MRI agent, and PTX as the anticancer drug to prepare the target modified theranostic PTX/SPIO-SSL-$H_7K(R_2)_2$.

Table 2 The IC_{50} values of PTX-SSL-$H_7K(R_2)_2$ in MDA-MB-231 cells (n=3)

PTX formulations	IC_{50} (μM)	
	pH 7.4	pH 6.8
Taxol	6.07±0.07	5.22±0.05
PTX-SSL	31.92±4.08	36.78±3.48
PTX-SSL-$H_7K(R_2)_2$	31.97±4.94	7.24±0.57**

Note: **$p<0.01$ versus that at pH 7.4.
Abbreviations: PTX, paclitaxel; PTX/SPIO-SSL-$H_7K(R_2)_2$, $H_7K(R_2)_2$-modified liposome containing PTX and SPIO; PTX-SSL, sterically stabilized liposome containing PTX; SSL, sterically stabilized liposome.

The targeting effect, MRI, and antitumor activity of PTX/SPIO-SSL-$H_7K(R_2)_2$ were investigated in detail in vitro and in vivo.

It has been reported that many conjugated ligands have been used for modifying theranostic nanomedicines for targeting tumor overexpressed receptor.[32] Here, we selected $H_7K(R_2)_2$, a tumor-specific, pH-responsive peptide, as the targeting ligand which could respond at an acidic tumor microenvironment by exhibiting CPP characteristics. We previously proved that $H_7K(R_2)_2$ could respond to acidic pH in MCF-7, C6, and U87 MG cell lines.[23,24] In this research, the tumor-specific, pH-responsive characteristic of $H_7K(R_2)_2$ was also confirmed in MDA-MB-231 cell line in vitro (Figure 3) and in vivo (Figure 4), showing its extensive targeting effect for responsive tumor acidic microenvironment. The PTX/SPIO-SSL-$H_7K(R_2)_2$ could only respond to acidic pH and produce targeting effect in tumor acidic microenvironment, not depending on the tumor cell overexpressed receptor, and showing a wide range of targeting effects. Our in vitro release results (Figure 2) indicated that the $H_7K(R_2)_2$ on the liposome surface does not destabilize the liposomal bilayer structure at an acidic pH, similar to our previous report.[23,24]

SPIO NPs were prepared by alkaline co-precipitation method following our previously described method.[25] Our previous results indicated that the prepared SPIO NPs exhibited superparamagnetic characteristics and had desirable features for MRI. Therefore, in this research, we used SPIO NPs as the MRI diagnostic agent to prepare theranostic PTX/SPIO-SSL-$H_7K(R_2)_2$.

PTX, one of the most successful anticancer drugs in clinical use, exhibits high antitumor activity against a wide range of tumors, including breast cancer.[33] Here, we selected PTX as the therapeutic drug to prepare the theranostic PTX/SPIO-SSL-$H_7K(R_2)_2$. The antitumor activity of PTX/SPIO-SSL-$H_7K(R_2)_2$ on human breast carcinoma MDA-MB-231 was confirmed in vitro and in vivo.

It is well known that liposome has been developed as a nanocarrier for theranostic application.[13] Liposome, the most clinically established nanometer-scale system, could entrap both lipophilic and hydrophobic compounds in a lipid membrane and aqueous core. Liposome surface can be easily conjugated with targeting molecules. Liposome could accumulate in the tumor tissues by passive targeting, or by active targeting of cancer cell or angiogenic marker specifically (liposome surface could be easily modified with targeting molecules).[34] Many theranostic liposomes have been reported for therapy and diagnosis, such as topotecan-loaded liposome-containing quantum dots (L-QD-TPT)[35]

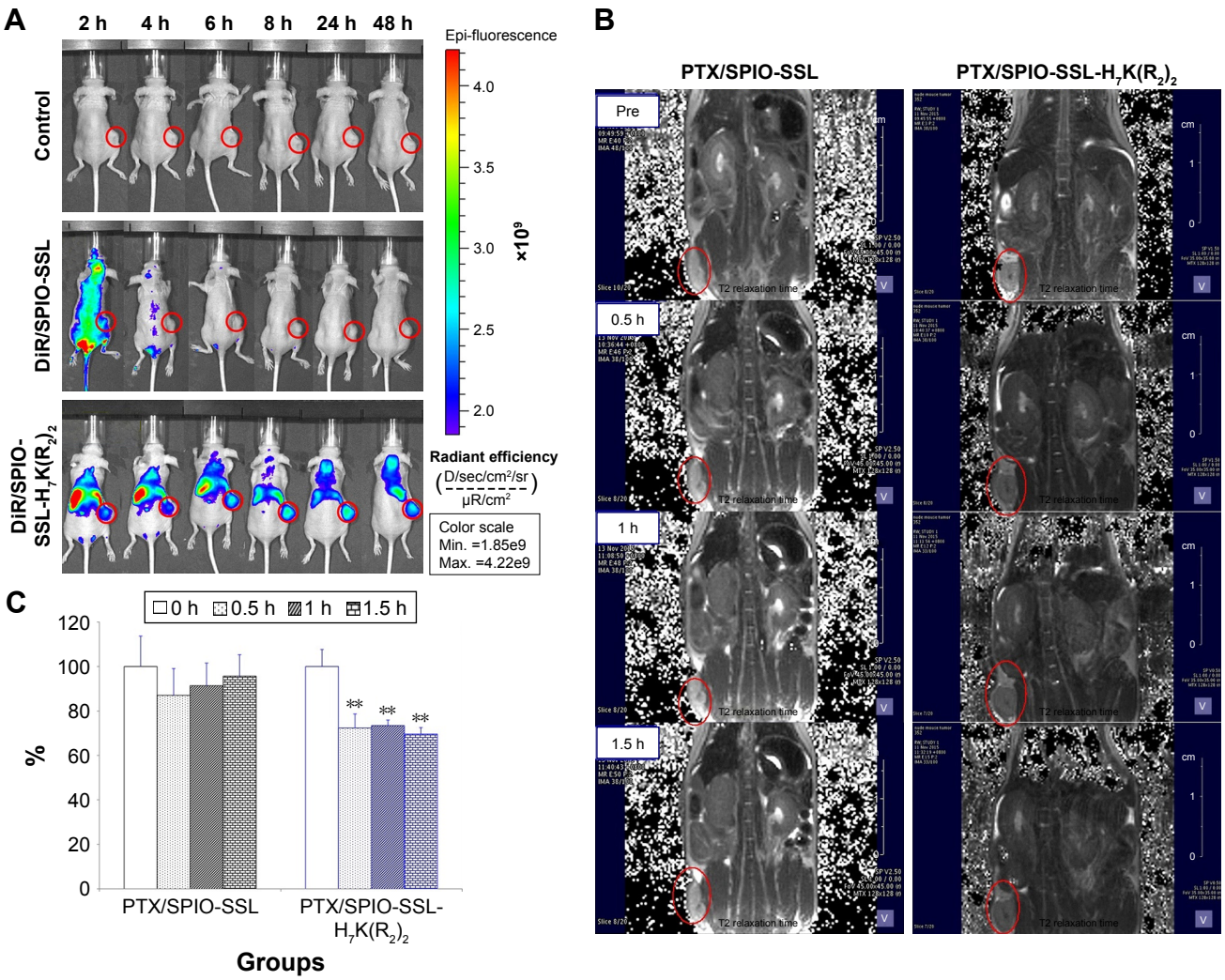

Figure 4 Tissue distribution and in vivo MRI of magnetoliposomes in MDA-MB-231 tumor-bearing mice.

Notes: (**A**) Tissue distribution of DiR-loaded liposomes in tumor-bearing mice. In vivo imaging of MDA-MB-231 tumor-bearing mice after 5% glucose solution (as control), DiR/SPIO-SSL, and DiR/SPIO-SSL-$H_7K(R_2)_2$ administration at 2, 4, 6, 8, 24, and 48 h, respectively. (**B**) In vivo MRI of MDA-MB-231 tumor model. In vivo MRI of MDA-MB-231 tumor-bearing mice after PTX/SPIO-SSL and PTX/SPIO-SSL-$H_7K(R_2)_2$ administration at 0, 0.5, 1, and 1.5 h, respectively. (**C**) Quantitative T_2 measurements in in vivo MRI of MDA-MB-231 tumor model. Quantitative T_2 measurements showed ~30%±3% decrease of PTX/SPIO-SSL-$H_7K(R_2)_2$ group at 0.5, 1, and 1.5 h. $^{**}p<0.01$ versus that of preinjection of liposomes (0 h time point) as control.

Abbreviations: DiR, 1,10-dioctadecyltetramethyl indotricarbocyanine iodide; MRI, magnetic resonance imaging; PTX, paclitaxel; PTX/SPIO-SSL, PTX/SPIO-loaded liposome; PTX/SPIO-SSL-$H_7K(R_2)_2$, $H_7K(R_2)_2$-modified liposome containing PTX and SPIO; SPIO, superparamagnetic iron oxide; SSL, sterically stabilized liposome.

and SPIO NPs coated with liposome-containing indocyanine green modified with a tumor-targeted agent RGD (SPIO@Liposome-ICG-RGD).[36] In our prepared theranostic PTX/SPIO-SSL-$H_7K(R_2)_2$, PTX was encapsulated in lipid bilayer, SPIO NPs were encapsulated in liposomal aqueous core, and $H_7K(R_2)_2$ as the targeting molecule was on the liposome surface.

Considering the results of in vivo MRI and in vivo antitumor activity of PTX/SPIO-SSL-$H_7K(R_2)_2$, we conclude that we have developed targeting modified theranostic liposomes which contain both the antitumor agent PTX and the MRI diagnostic agent SPIO NPs for antitumor therapy and MRI.

Conclusion

The tumor-specific, pH-responsive, peptide-modified, theranostic liposome-containing PTX and SPIO NPs, PTX/SPIO-SSL-$H_7K(R_2)_2$, was developed for the co-delivery of MRI agent SPIO NPs and therapeutic agent PTX. Both SPIO NPs and PTX were encapsulated into liposome by thin film hydration. The targeting effect, MRI, and antitumor activity of PTX/SPIO-SSL-$H_7K(R_2)_2$ were confirmed in in vitro and in vivo experiments. Considering all our in vitro and in vivo results, we conclude that we developed targeting modified theranostic liposomes which could achieve both antitumor activity and MRI.

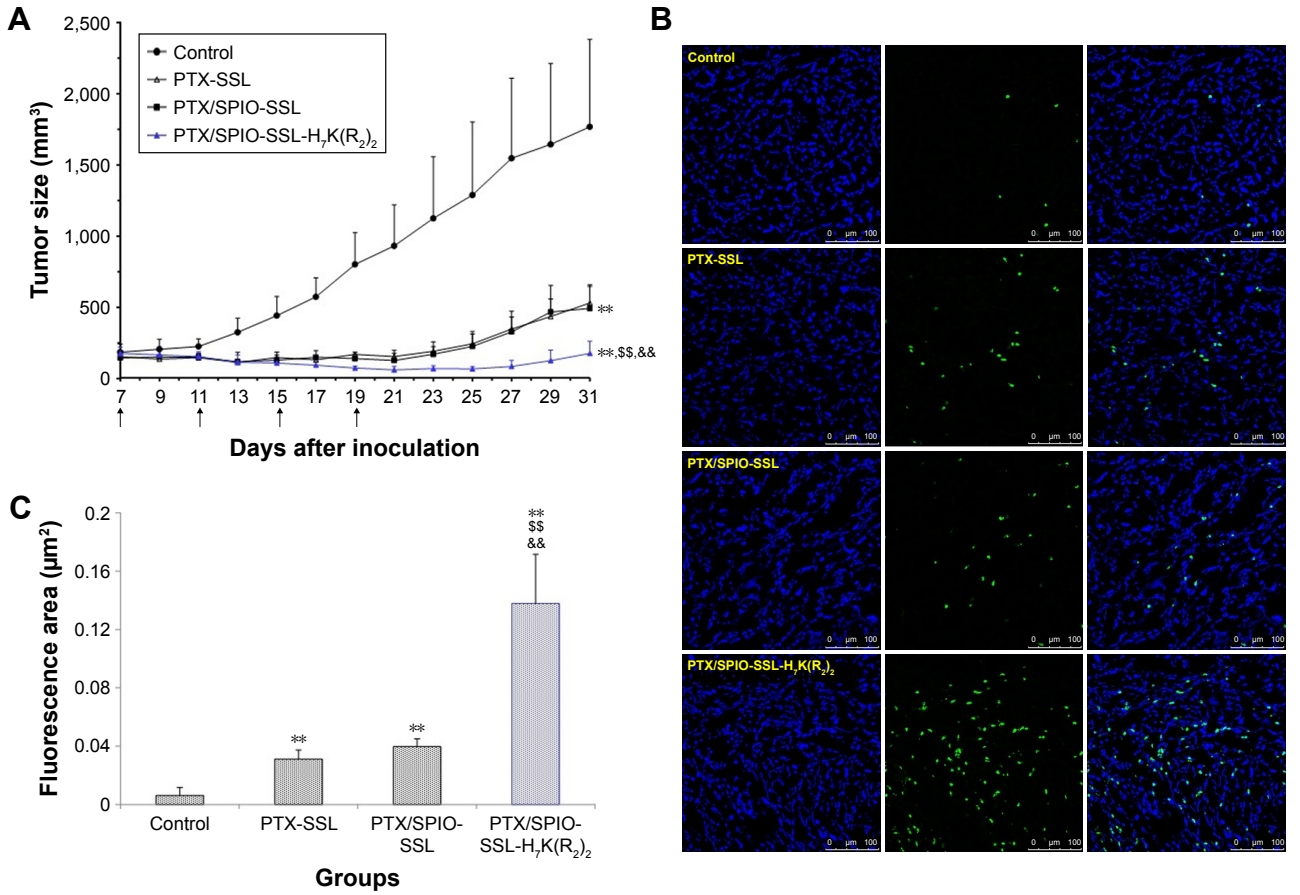

Figure 5 In vivo antitumor activity of PTX/SPIO-SSL-$H_7K(R_2)_2$.

Notes: BALB/C nude mice were inoculated s.c. with MDA-MB-231 cells and treated with 5% glucose solution, PTX-SSL (15 mg/kg, i.v., q4d), PTX/SPIO-SSL (15 mg/kg, i.v., q4d), and PTX/SPIO-SSL-$H_7K(R_2)_2$ (15 mg/kg, i.v., q4d), respectively. For each administration, formulations were given to mice via the tail vein. (**A**) Tumor growth inhibition. (**B**) TUNEL staining of the tumor tissue sections was performed according to the standard protocols provided by the manufacturers. The apoptotic cells were detected by TUNEL. DNA strand breaks were labeled green, and the nuclei were stained with Hoechst 332589 (blue). Apoptotic cells exhibited a turquoise color as a result of color merging of these two labels. (**C**) The fluorescence area of each group was used for the statistical analysis of apoptosis activity. $^{**}p<0.01$ versus the 5% glucose solution treatment group as a control; $^{\$\$}p<0.01$ versus the PTX-SSL treatment group; $^{\&\&}p<0.01$ versus the PTX/SPIO-SSL treatment group.

Abbreviations: i.v., intravenous; PTX, paclitaxel; PTX/SPIO-SSL, PTX/SPIO-loaded liposome; PTX/SPIO-SSL-$H_7K(R_2)_2$, $H_7K(R_2)_2$-modified liposome containing PTX and SPIO; PTX-SSL, sterically stabilized liposome containing PTX; q4d, twice a day for 4 days; s.c., subcutaneously; SPIO, superparamagnetic iron oxide; TUNEL, terminal deoxynucleotidyl transferase dUTP nick end labeling.

Acknowledgments

The authors alone are responsible for the content and writing of this article. The authors gratefully acknowledge the financial support from the National Key Research and Development Program of China (2017YFA0205600).

Disclosure

The authors report no conflicts of interest in this work.

References

1. Ryu JH, Koo H, Sun IC, et al. Tumor-targeting multi-functional nanoparticles for theragnosis: new paradigm for cancer therapy. *Adv Drug Deliv Rev*. 2012;64(13):1447–1458.
2. Schleich N, Danhier F, Préat V. Iron oxide-loaded nanotheranostics: major obstacles to in vivo studies and clinical translation. *J Control Release*. 2015;198:35–54.
3. Hahn MA, Singh AK, Sharma P, Brown SC, Moudgil BM. Nanoparticles as contrast agents for in-vivo bioimaging: current status and future perspectives. *Anal Bioanal Chem*. 2011;399(1):3–27.
4. Bennett KM, Jo J, Cabral H, Bakalova R, Aoki I. MR imaging techniques for nano-pathophysiology and theranostics. *Adv Drug Deliv Rev*. 2014;74:75–94.
5. Roy Chowdhury M, Schumann C, Bhakta-Guha D, Guha G. Cancer nanotheranostics: strategies, promises and impediments. *Biomed Pharmacother*. 2016;84:291–304.
6. Schleich N, Danhier F, Préat V. Iron oxide-loaded nanotheranostics: major obstacles to in vivo studies and clinical translation. *J Control Release*. 2015;198:35–54.
7. Gobbo OL, Sjaastad K, Radomski MW, Volkov Y, Prina-Mello A. Magnetic nanoparticles in cancer theranostics. *Theranostics*. 2015;5(11):1249–1263.
8. Kandasamy G, Maity D. Recent advances in superparamagnetic iron oxide nanoparticles (SPIONs) for in vitro and in vivo cancer nanotheranostics. *Int J Pharm*. 2015;496(2):191–218.
9. Mahmoudi M, Sant S, Wang B, Laurent S, Sen T. Superparamagnetic iron oxide nanoparticles (SPIONs): development, surface modification and applications in chemotherapy. *Adv Drug Deliv Rev*. 2011;63(1–2):24–46.

10. Zhou H, Qian W, Uckun FM, et al. IGF1 receptor targeted theranostic nanoparticles for targeted and image-guided therapy of pancreatic cancer. *ACS Nano*. 2015;9(8):7976–7991.
11. Zarrin A, Sadighian S, Rostamizadeh K, et al. Design, preparation, and in vitro characterization of a trimodally-targeted nanomagnetic onco-theranostic system for cancer diagnosis and therapy. *Int J Pharm*. 2016;500(1–2):62–76.
12. Wang D, Fei B, Halig LV, et al. Targeted iron-oxide nanoparticle for photodynamic therapy and imaging of head and neck cancer. *ACS Nano*. 2014;8(7):6620–6632.
13. Xing H, Hwang K, Lu Y. Recent developments of liposomes as nanocarriers for theranostic applications. *Theranostics*. 2016;6(9):1336–1352.
14. Clares B, Biedma-Ortiz RA, Sáez-Fernández E, et al. Nano-engineering of 5-fluorouracil-loaded magnetoliposomes for combined hyperthermia and chemotherapy against colon cancer. *Eur J Pharm Biopharm*. 2013;85(3 Pt A):329–338.
15. Chen Y, Chen Y, Xiao D, Bose A, Deng R, Bothun GD. Low-dose chemotherapy of hepatocellular carcinoma through triggered-release from bilayer-decorated magnetoliposomes. *Colloids Surf B Biointerfaces*. 2014;116:452–458.
16. Di Corato R, Béalle G, Kolosnjaj-Tabi J, et al. Combining magnetic hyperthermia and photodynamic therapy for tumor ablation with photoresponsive magnetic liposomes. *ACS Nano*. 2015;9(3):2904–2916.
17. Guo H, Chen W, Sun X, Liu YN, Li J, Wang J. Theranostic magnetoliposomes coated by carboxymethyl dextran with controlled release by low-frequency alternating magnetic field. *Carbohydr Polym*. 2015;118:209–217.
18. Zhang L, Zhou H, Belzile O, Thorpe P, Zhao D. Phosphatidylserine-targeted bimodal liposomal nanoparticles for in vivo imaging of breast cancer in mice. *J Control Release*. 2014;183:114–123.
19. Tian Y, Zhang Y, Teng Z, et al. pH-Dependent transmembrane activity of peptide-functionalized gold nanostars for computed tomography/photoacoustic imaging and photothermal therapy. *ACS Appl Mater Interfaces*. 2017;9(3):2114–2122.
20. Farkhani SM, Valizadeh A, Karami H, Mohammadi S, Sohrabi N, Badrzadeh F. Cell penetrating peptides: efficient vectors for delivery of nanoparticles, nanocarriers, therapeutic and diagnostic molecules. *Peptides*. 2014;57:78–94.
21. Shi K, Li J, Cao Z, et al. A pH-responsive cell-penetrating peptide-modified liposomes with active recognizing of integrin αvβ3 for the treatment of melanoma. *J Control Release*. 2015;217:138–150.
22. Schach DK, Rock W, Franz J, Bonn M, Parekh SH, Weidner T. Reversible activation of a cell-penetrating peptide in a membrane environment. *J Am Chem Soc*. 2015;137(38):12199–12202.
23. Zhao BX, Zhao Y, Huang Y, et al. The efficiency of tumor-specific pH-responsive peptide-modified polymeric micelles containing paclitaxel. *Biomaterials*. 2012;33(8):2508–2520.
24. Zhao Y, Ren W, Zhong T, et al. Tumor-specific pH-responsive peptide-modified pH-sensitive liposomes containing doxorubicin for enhancing glioma targeting and anti-tumor activity. *J Control Release*. 2016;222:56–66.
25. Ren W, Zhang S, Zhong T, et al. The preparation and characteristics of sterically stabilized liposomes containing paclitaxel and superparamagnetic iron oxide nanoparticles. *J Chin Pharm Sci*. 2016;25(8):570–575.
26. Luo LM, Huang Y, Zhao BX, et al. Anti-tumor and anti-angiogenic effect of metronomic cyclic NGR-modified liposomes containing paclitaxel. *Biomaterials*. 2013;34(4):1102–1114.
27. Liu XR, Wu KC, Huang Y, et al. In vitro and in vivo studies on plasma-to-blood ratio of paclitaxel in human, rabbit and rat blood fractions. *Biol Pharm Bull*. 2008;31(6):1215–1220.
28. Huang D, Zhang S, Zhong T, et al. Multi-targeting NGR-modified liposomes recognizing glioma tumor cells and vasculogenic mimicry for improving anti-glioma therapy. *Oncotarget*. 2016;7(28):43616–43628.
29. Song P, Yao X, Zhong T, et al. The anti-tumor efficacy of 3-(2-Nitrophenyl) propionic acid-paclitaxel (NPPA-PTX): a novel paclitaxel bioreductive prodrug. *Oncotarget*. 2016;7(30):48467–48480.
30. Zhong T, Yao X, Zhang S, et al. A self-assembling nanomedicine of conjugated linoleic acid-paclitaxel conjugate (CLA-PTX) with higher drug loading and carrier-free characteristic. *Sci Rep*. 2016;6:36614.
31. Guo Y, Zhong T, Duan XC, et al. Improving anti-tumor activity of sorafenib tosylate by lipid- and polymer-coated nanomatrix. *Drug Deliv*. 2017;24(1):270–277.
32. Ramzy L, Nasr M, Metwally AA, Awad GAS. Cancer nanotheranostics: a review of the role of conjugated ligands for overexpressed receptors. *Eur J Pharm Sci*. 2017;104:273–292.
33. Zong Y, Wu J, Shen K. Nanoparticle albumin-bound paclitaxel as neoadjuvant chemotherapy of breast cancer: a systematic review and meta-analysis. *Oncotarget*. 2017;8(10):17360–17372.
34. Dai Z, Yue X. Liposomal nanotechnology for cancer theranostics. *Curr Med Chem*. Epub 2017 Mar 5.
35. Seleci M, Ag Seleci D, Scheper T, Stahl F. Theranostic liposome-nanoparticle hybrids for drug delivery and bioimaging. *Int J Mol Sci*. 2017;18(7):E1415.
36. Chen Q, Shang W, Zeng C, et al. Theranostic imaging of liver cancer using targeted optical/MRI dual-modal probes. *Oncotarget*. 2017;8(20):32741–32751.